DNA-Templated Semiconductor Nanocrystal Growth for Controlled DNA Packing and Gene Delivery

Li Gao and Nan Ma*

CAS Key Laboratory of Health Informatics, Institute of Biomedicine and Biotechnology, Shenzhen Institutes of Advanced Technology, Chinese Academy of Sciences, Shenzhen, 518055, People's Republic of China

ABSTRACT

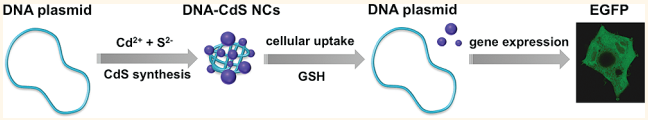

DNA-templated semiconductor nanocrystal (SNC) growth represents a facile means to generate bioactive hybrid nanostructures by directly integrating DNA molecules and luminescent SNCs together *via* a one-step synthesis, which has been applied to biosensing and cell imaging. In this study we for the first time demonstrated that DNA-templated CdS SNC growth could also be used to rationally tune the structures and activities of large DNA molecules. We explored the synergistic effects of nanocrystal growth on the sizes and charges of DNA molecules and demonstrate that the CdS growth-induced DNA packing could be used as a smart gene delivery system. Herein we used DNA plasmids encoding intact enhanced green fluorescence protein (EGFP) genes as templates to grow CdS SNCs and found that the stepwise growth of CdS nanocrystals can spontaneously induce DNA condensation and negative charge shielding in a synergistic manner. The condensed DNA plasmids exhibited efficient cellular uptake and a relative gene transfection efficiency of 32%. The transfection efficiency can be further doubled in the presence of chloroquine. We elucidated that the gene transfection and expression is controlled by reversible DNA packing, where ligand exchange of DNA with intracellular glutathione molecules plays a critical role in the recovery of DNA plasmids for gene expression.

KEYWORDS: semiconductor nanocrystals · nanostructures · biotemplated synthesis · nucleic acids · gene delivery

Biomolecules possessing sophisticated nanostructures are widely exploited to synthesize a variety of functional nanomaterials with precise bottom-up control.[1−8] While many studies have been focused on programming the physical pro perties and assembly of as-prepared inorganic nanomaterials *via* designer biomolecules, the synergistic effects of biotemplated synthesis on a biomolecule itself—a new means to rationally control the structures and activities of biomolecules *via* biotemplated inorganic nanomaterial scaffold interfacing—remain little explored.

Nucleic acid molecules are superior ligands for aqueous synthesis of semiconductor nanocrystals (SNCs) owing to their high capacity for metal ion sequestration, nanocrystal nucleation, and passivation.[9−12] Within the DNA−SNC hybrid nanostructures DNA molecules lie on the nanocrystal surfaces *via* multidentate bonding to reach maximum surface passivation and minimum hydrodynamic size. Discrete, small DNA motifs containing 25 nucleotides (sub-10 nm) have been previously used to synthesize SNCs to generate bioactive hybrid nanostructures for biosensing and cancer cell targeting, which represents a facile strategy to directly integrate DNA bioactivity and SNC photoluminescence into a single nanostructure *via* a one-step synthesis.[13] Large DNA molecules encoding intact genes are of particular interest owing to their high potential for gene modification and therapy. These naked DNA molecules cannot enter host cells by themselves but have to complex with some transfection reagents such as cationic polymers or lipids for gene delivery due to their large sizes (over 500 nm) and high density of negative charge. In this study we present a novel gene delivery strategy based on rationally controlling the packing and unpacking of DNA plasmids *via* DNA-templated growth of inorganic SNC scaffolds (Scheme 1). We envision that direct growing SNCs along DNA molecules would spontaneously induce DNA curvature and condensation as well as negative charge shielding, which are favorable for cellular internalization, while the intracellular restoration of DNA plasmids can be realized *via* a glutathione (GSH)-mediated ligand exchange process.

RESULTS AND DISCUSSION

As a proof-of-principle study, we employ DNA-templated CdS SNC growth as a platform for gene delivery study since the

* Address correspondence to nan.ma@siat.ac.cn.

Received for review October 28, 2011 and accepted December 21, 2011.

Published online December 21, 2011
10.1021/nn204162y

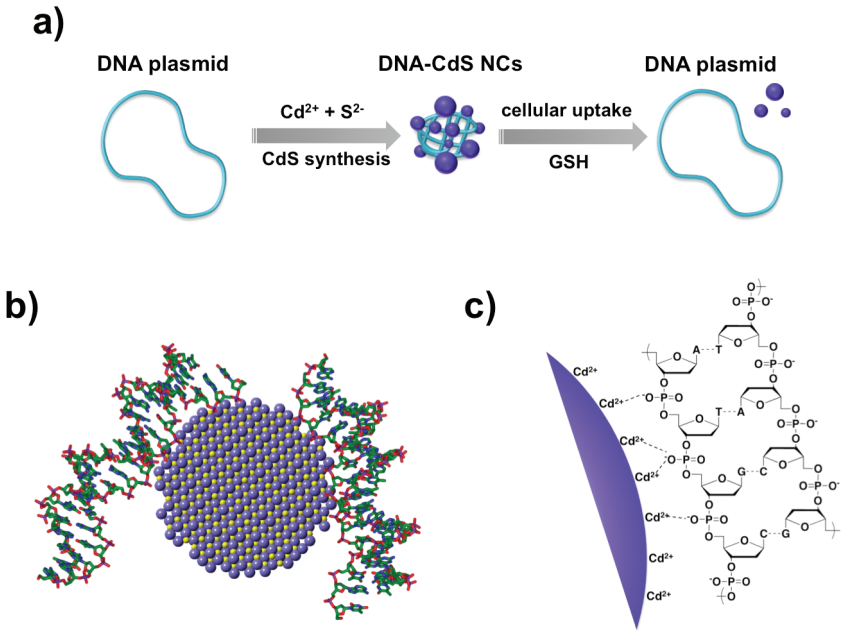

Scheme 1. Schematic illustration of DNA plasmid-templated CdS NCs growth. (a) CdS NC growth along DNA plasmid induced DNA packing and GSH-mediated DNA unpacking. (b) Schematic illustration of the double-stranded DNA–CdS NC hybrid nanostructure. (c) Electrostatic interaction between phosphate backbone and surface Cd^{2+} ions.

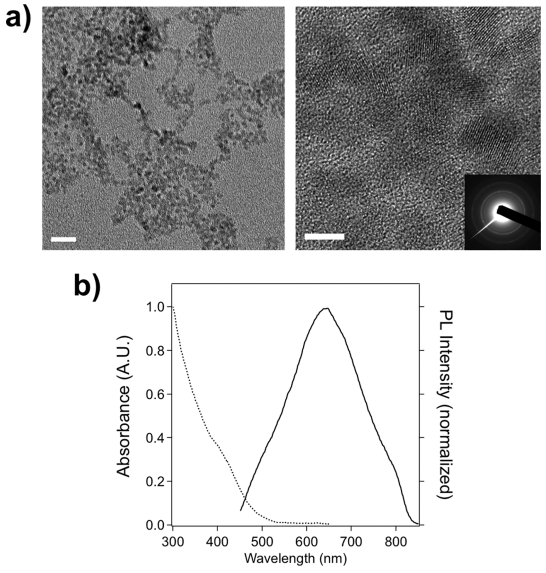

Figure 1. Nanocharacterization and optical characterization of CdS NCs grown on DNA plasmids. (a) Low-magnification (left) and high-magnification (right) images of as-prepared CdS NCs. The inset is selected area diffraction (SAD) of CdS NCs. The scale bars on the left image and right image are 20 and 5 nm, respectively. (b) Absorption and photoluminescence spectra of DNA-templated CdS NCs.

synthesis can be easily processed at ambient conditions and the interactions between DNA and CdS have been elucidated. The DNA-templated CdS growth usually involves two steps. The first step is the binding of the cadmium ions with the negatively charged DNA backbones to form a supersaturated microenvironment, which would facilitate heterogeneous nucleation; the second step is the formation of CdS nuclei and subsequent growth to form nanocrystals upon the introduction of the sulfide ions.[1] In this study a double-stranded DNA plasmid pEGFP-N1 (4733 bp) encoding EGFP was selected for SNC synthesis so that the gene delivery can be monitored by intracellular EGFP expression using fluorescence microscopy. For CdS SNC synthesis, Cd^{2+} and S^{2-} ions were injected into DNA solution sequentially to promote nanocrystal nucleation and growth. A nucleobase to Cd^{2+} to S^{2-} ratio of 3:2:1 and a Cd^{2+} concentration of 500 μM were chosen to produce CdS nanocrystals with Cd^{2+}-rich surfaces and optimized luminescence intensity. The reaction solution turned yellow immediately upon the addition of S^{2-} ions, indicating the formation of CdS nanoparticles. These nanoparticles can be easily visualized in TEM images, and the lattice fringes observed in high-resolution TEM (HRTEM) images confirm that the particles are crystalline materials (Figure 1a). Most of CdS nanoparticles have an oblate shape with an aspect ratio between 1.1 and 1.8; the mean diameter along the short dimension is 4.0 ± 0.6 nm. The absorption and photoluminescence spectra of the as-prepared CdS nanocrystals are shown in Figure 1b. The photoluminescence spectrum ranging from 500 to 800 nm is characteristic of trap state emission originating from the surface defects. The quantum yield (QY) of the CdS nanocrystals was 2.5%. A control experiment was conducted under the same conditions in the absence of DNA molecules; however, only nonluminescent bulk materials were generated, which can be easily removed *via* centrifugation. These results suggest that DNA molecules play a critical role in nanocrystal formation and stabilization. Since the base moieties of

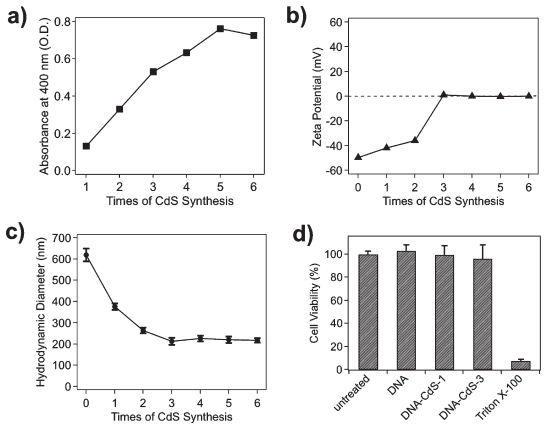

Figure 2. (a–c) DNA-templated CdS NC growth-induced DNA condensation and charge shielding. Six sequential CdS syntheses were conducted. CdS absorbance at 400 nm (a), DNA–CdS zeta-potential (b), and DNA–CdS hydrodynamic diameter (c) were monitored as a function of rounds of CdS synthesis. (d) Cytotoxicity of DNA–CdS hybrid nanostructures with live 293T cells. Naked DNA plasmids and three DNA–CdS samples with one and three rounds of CdS synthesis were tested. Untreated and Triton-X 100-treated 293T cells were used as negative control and positive control, respectively.

double-stranded DNA plasmids were tethered by hydrogen bonding and hence are not available for nanocrystal passivation, the interaction between CdS nanocrystals and DNA molecules is mainly through electrostatic interaction between surface Cd^{2+} ions and negatively charged oxygen atoms on the phosphate backbones. This DNA plasmid-templated semiconductor nanocrystal synthesis strategy can be extended to CdTe NCs, which possess better optical properties. The synthesis of plasmid–CdTe NC complex is derived from a protocol we previously reported for discrete, small DNA motif templates. The as-prepared CdTe NCs possess a narrow band-edge emission peak (fwhm = 50 nm) (Figure S1) and a high QY (21%), which would be better suited for cellular trafficking.

For gene delivery study, we first explore whether the DNA-templated CdS NCs can serve as scaffolds to effectively condense DNA plasmids and shield their negative charges by monitoring the zeta-potentials and hydrodynamic diameters (HD) of DNA plasmids before and after the synthesis of CdS NCs. As shown in Figure 2, after the first CdS synthesis, the zeta-potential of DNA plasmids shifted from −50 mV to −42 mV and the average HD decreased from 619 ± 30 nm to 376 ± 14 nm, indicating partial neutralization of DNA negative charges and condensation of DNA plasmids. The remaining negative charges suggest that there are still some sites on DNA phosphate backbones available for CdS NCs growth and passivation. In order to further compact DNA plasmids and shield their negative charges, we conducted more syntheses of CdS NCs using the same conditions as the first synthesis. The production of CdS NCs was monitored by their absorbance at 400 nm. As shown in Figure 2a, six syntheses of CdS NCs were conducted sequentially, and there was a stepwise increase of CdS products from the first synthesis to the fifth synthesis, until which the saturation of DNA templates for NCs growth was reached. It should be noted that the multistep synthesis of CdS NCs could not be replaced by a one-step synthesis using elevated precursor concentrations, which can significantly affect the growth kinetics of NCs and result in the formation of insoluble bulk materials. The changes of zeta-potential and HD of DNA plasmids as a function of rounds of CdS NCs synthesis are shown in Figure 2b and c. The zeta-potential gradually increased and became zero after the third synthesis, revealing complete neutralization of all the negative charges of DNA plasmids. More NC synthesis did not further alter the zeta-potential. Meanwhile, the HD of DNA plasmids gradually decreased as more CdS syntheses were conducted. A minimum HD of 213 ± 16 nm, which corresponds to the highest condensation capacity, was reached after the third CdS synthesis. The HD remained almost constant for further CdS synthesis. The ratio of number of CdS NCs to plasmids for three rounds of CdS synthesis was estimated to be 12. It has been shown that the particles with a diameter of 200 nm were endocytosed much more efficiently than the particles with a diameter of 500 nm.[14] Therefore, the condensation of DNA plasmids would be more favorable for cellular internalization and gene delivery. Our results suggest that at least three rounds of CdS NC synthesis are required to effectively compact DNA plasmids and shield their negative charges. The good correlation between zeta-potential increase and HD decrease indicates that NC growth-induced charge shielding and DNA packing are synergistic.

The cytotoxicity of DNA–CdS hybrid nanostructure was evaluated using the MTT assay. Three samples including naked DNA plasmids and DNA plasmids with one (DNA–CdS-1) and three (DNA–CdS-3) syntheses of CdS NCs were tested, and the dosage was kept the same as in transfection studies (4×10^{-3} μg/μL DNA plasmid). Live 293T cells were incubated with DNA or DNA–CdS for 5 h, after which the medium was replaced with fresh DMEM and the cells were cultured for 48 h before toxicity measurements. As shown in Figure 2d, all the tested samples had little effect on the cell viabilities, implying that these DNA–CdS nanostructures are compatible for transfection experiments. The CdS NC concentrations of DNA–CdS-1 and DNA–CdS-3 samples were 4 and 15 nM, respectively, determined according to CdS absorbance at the first excitonic absorption peak.[15] Previous studies show that the DNA-templated CdS and CdTe QDs with a much higher concentration (70–200 nM) were nontoxic to a variety of cell lines.[10,13] Therefore, the very low concentration of CdS NCs used in this study is not likely to cause severe toxicity.

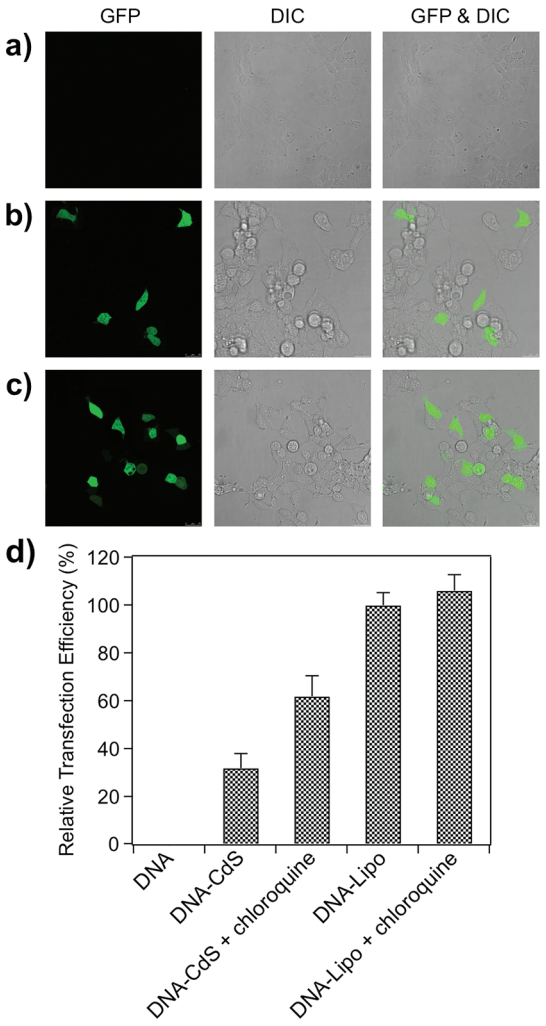

Figure 3. Confocal microscopy of EGFP expression in 293T cells transfected with (a) naked DNA plasmid, (b) DNA–CdS-3, and (c) DNA–Lipo (DIC: differential interference contrast). (d) Relative transfection efficiency of 293T cells transfected with DNA plasmid, DNA–CdS-3, DNA–CdS-3 with chloroquine, DNA–Lipo, and DNA–Lipo with chloroquine.

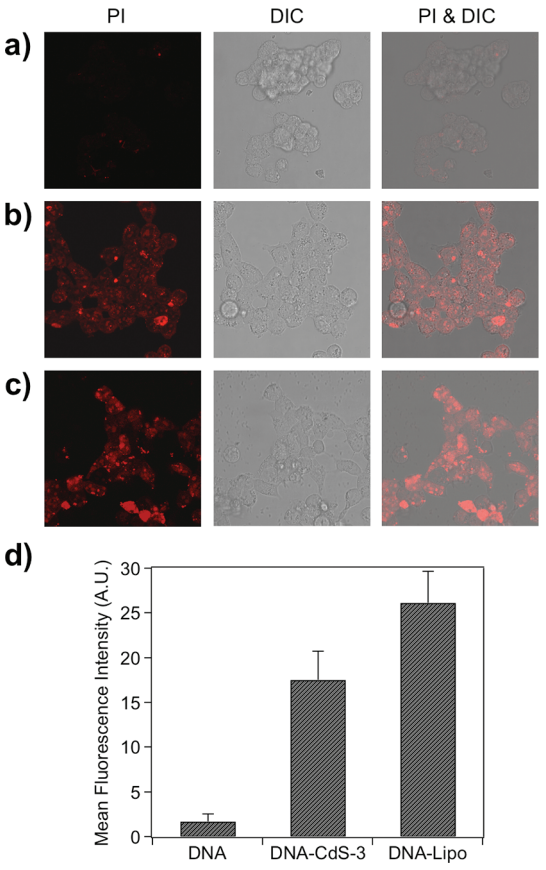

Figure 4. Confocal microscopy of cellular uptake of (a) PI-labeled DNA plasmid, (b) DNA–CdS-3, and (c) DNA–Lipo. (d) Mean fluorescence intensity of 293T cells incubated with PI-labeled DNA plasmid, DNA–CdS-3, and DNA–Lipo.

For transfection experiments, the pEGFP-N1 DNA plasmids with three syntheses of CdS NCs (DNA–CdS-3) were incubated with 293T cells for 5 h at 37 °C, after which the cell medium containing DNA–CdS was replaced with fresh medium and the cells were further cultured for a period of 48 h at 37 °C to allow EGFP expression. Transfection with naked DNA plasmids and Lipofectamine 2000-complexed DNA plasmids were used as negative and positive controls, respectively. As shown in Figure 3 and Figure S2, both the transfections with DNA–CdS and DNA–Lipofectamine 2000 (DNA–Lipo) lead to EGFP expression in a fraction of 293T cells, whereas transfection with naked DNA plasmids did not produce any EGFP expression. The relative transfection efficiency (100% for DNA–Lipo) of DNA–CdS was 32%. The absolute transfection efficiencies for DNA–Lipo and DNA–CdS were 33% and 10%, respectively. The distinct results for naked DNA plasmids and DNA–CdS hybrid nanostructures imply that the DNA condensation and charge shielding induced by DNA-templated CdS NCs growth probably facilitate the entry of DNA plasmids into live cells, which finally leads to gene expression in the nucleus. To further elucidate the cellular uptake and intracellular trafficking of DNA–CdS and DNA–Lipo, we labeled DNA molecules with propidium iodide (PI), a fluorophore that exhibits enhanced fluorescence (20–30-fold) by DNA intercalation. Fluorescence spectra of PI-labeled DNA and DNA–CdS are shown in Figure S3. PI alone does not emit detectable fluorescence and is excluded from live cells, so the red fluorescence signals in live cells originated from the internalized PI-labeled DNA plasmids. An excitation wavelength of 543 nm was selected for PI molecules. As shown in Figure 4, there is very little fluorescence from the cells incubated with PI-labeled naked DNA plasmids, indicating that the naked DNA plasmids can hardly enter cells. In contrast, a 10-fold increase of mean fluorescence intensity was observed for the cells incubated with PI-labeled DNA–CdS-3 hybrid nanostructures, suggesting efficient uptake of this material. The uptake efficiency (mean fluorescence intensity) of DNA–CdS-3 is 67% of DNA–Lipo complex (Figure 4d). DNA–CdS with one and two rounds of CdS synthesis can also enter cells, yet to a lesser extent (Figure S4).

A good correlation between the cellular uptake of DNA–CdS and the degree of plasmid condensation and charge shielding can be identified (Figure S4e). By co-localizing with Lysotracker Green we found that the DNA–CdS hybrid nanostructures were internalized *via* an endocytic pathway and trapped into late endosomes and lysosomes (SI Figure S5). While cationic lipids were able to destabilize endosomal membranes and facilitate endosomal escape of DNA molecules,[16] it is unclear whether DNA–CdS could escape from endosomes efficiently, which would be a limiting factor that affects the overall transfection efficiency. This is elucidated by treating the cells with chloroquine, a compound that is known to facilitate endosomal escape of endocytosed species.[17] About 2-fold increase of transfection efficiency was observed when the cells were incubated with both DNA–CdS and chloroquine (Figure 3d and Figure S2). Conversely, only a slight increase of transfection efficiency was observed for the cells transfected with DNA–Lipo and chloroquine, suggesting that the endosomal escape is unlikely a limiting factor in transfection efficiency for the DNA–Lipo complex. Also, intracellular restoration of the DNA transcriptional activity is a prerequisite for EGFP expression. To elucidate this, Leong and Wang have developed a FRET-based strategy using quantum dot–fluorophore pairs to track intracellular unpacking of DNA plasmids that complex with chitosan.[18] We reason that in our study the recovery of DNA plasmids could be achieved *via* an intracellular ligand exchange process between DNA molecules and thiol-containing moieties because thiol group can strongly bind to a Cd^{2+} ion and interrupt the interaction between the DNA phosphate backbone and the Cd^{2+} ion. Glutathione (GSH) is the most abundant thiol-containing molecule in live cells (2–10 mM) and is likely to play a critical role in DNA release. We demonstrated this by incubating 5 mM GSH with DNA–CdS at pH 7.5 for 1 h and monitoring the change of the DNA HD. After GSH treatment, the average HD of DNA plasmids increased from 217 nm to 636 nm, suggesting complete DNA unpacking. A pronounced red-shift of the photoluminescence spectrum of DNA–CdS was observed after GSH treatment (Figure S6), suggesting that the surface states of CdS NCs were altered by the interaction between GSH and the NC surface. Agarose gel electrophoresis was conducted to check whether the plasmids remain intact after GSH treatment. No change was observed for the unpacked plasmids in comparison with the original plasmids (Figure S7), indicating that the whole plasmid packing and unpacking process would not cause DNA damage.

CONCLUSION

In summary, we demonstrate a new means to tune the size and charges of large DNA molecules *via* DNA-templated growth of tiny inorganic CdS NCs. These NCs serve as scaffolds for DNA condensation and charge shielding. Furthermore, we elucidate that the NC growth-mediated DNA packing is a reversible process that can be used as a facile strategy for gene delivery. We believe that our study represents an essential step toward smart control over the structure and activity of biomolecules *via* inorganic nanomaterial interfacing, which would be valuable to the fabrication of novel nanobio systems in the future.

METHODS

Materials and Instrumentation. Cadmium chloride ($CdCl_2$, 99.996%) was purchased from Alfa Aesar. Sodium sulfide (Na_2S, 90%) was obtained from J&K Scientific Ltd. (Beijing). 3-(4,5-Dimethylthiazol-2-yl)-2,5-diphenyl-2*H*-tetrazolium bromide (MTT), propidium iodide, and chloroquine diphosphate salt were purchased from Sigma-Aldrich. Glutathione was obtained from Acros Organics. Lysotracker Green DND-26, Lipofectamine 2000, and plasmids pEGFP-N1 were purchased from Invitrogen. HEK 293T cells were purchased from American Type Culture Collection. Dulbecco's modified Eagle's medium (DMEM) and phosphate-buffered saline (PBS) were purchased from Gibco. Triton X-100 was purchased from Amresco. Water was purified with a Milli-Q water purification system. All other reagents and solvents were of analytical grade.

The fluorescence spectra and absorption spectra were recorded on a FSP 920 fluorometer and a PerkinElmer Lambda 25 absorption spectrophotometer, respectively. Zeta-potentials and hydrodynamic sizes were recorded on a Beckman Coulter Delsa Nano C particle analyzer. DNA plasmids were quantified on an Eppendorf Biophotometer Plus. Absorbance for the MTT assay was measured using a Biotek Synergy 4 plate reader. TEM images were taken on a JEOL JEM-2100 transmission electron microscope operating at 200 kV. Confocal microscopy was conducted on a Leica TCS SP5 II confocal microscope.

Preparation of DNA–CdS and DNA–CdTe Hybrid Nanostructures. For CdS NC synthesis, the molar ratio of nucleobase to cadmium to sulfur was set to 3:2:1. For a 200 μL synthesis, 150 nmol of DNA base and 100 nmol of $CdCl_2$ were added to a 1.5 mL Eppendorf tube and diluted to 150 μL with water. After incubating at room temperature for 5 min, 50 μL of a 10 mM Na_2S solution was quickly introduced into the DNA–$CdCl_2$ complex solution and intensely mixed *via* vortex agitation for 8 s. A light yellow solution was obtained immediately after the introduction of Na_2S. For the multistep synthesis, 100 nmol of $CdCl_2$ was added to the former product solution. After incubating at room temperature for 5 min, 5 μL of a 10 mM Na_2S solution was quickly introduced into the DNA–$CdCl_2$ complex solution and intensely mixed *via* vortex agitation for 8 s. This procedure was repeated for more syntheses. The DNA–CdS NCs constructs were purified using a Microcon centrifugal filter device (YM-30, Millipore) by centrifuging at 12 000 rpm for 20 min and recovering in distilled water. Quantum yields were measured using fluorescein in water as a standard. The ratio of number of CdS NCs to plasmids was determined by dividing the CdS NC concentration by the plasmid concentration. The CdS NC concentration was determined using an extinction coefficient reported by Peng *et al.*[15] For CdTe NC synthesis, sodium hydrogen telluride (NaHTe) was freshly made by reacting 0.025 g of sodium borohydride ($NaBH_4$) with 0.040 g of tellurium

powder in 1 mL of deionized water at room temperature overnight. 3-Mercaptopropionic acid (MPA) was used as co-ligand for the synthesis to ensure sufficient NC passivation. $CdCl_2$–MPA stock solution was made to include 1.25 mM $CdCl_2$ and 1.05 mM MPA in H_2O, and the pH was adjusted to 9.0 with sodium hydroxide before use. For a typical CdTe synthesis, 1 mL of $CdCl_2$–GSH stock solution was mixed with DNA solution containing 300 nmol of nucleobases in a 2 mL Eppendorf tube, and then 2 μL of freshly prepared NaHTe solution was introduced. The reaction was conducted on a heat block at 90 °C for 30 min and then gradually cooled to room temperature.

Transfection of DNA–CdS Hybrid Nanostructures. 293T cells were cultured on 25 cm^2 cell culture plates with vent caps (Corning) in DMEM supplemented with 10% fetal bovine serum (Hyclone) in a humidified incubator at 37 °C containing CO_2 (5%). 293T cells that had been grown to subconfluence were dissociated from the surface with a solution of 0.25% trypsin/EDTA (Hyclone) for 30 s. Then aliquots (300 μL, 4 $\times$ 10^4 cells) were seeded into an 8-well coverglass chamber (Nunc). After overnight incubation, the medium was replaced with 100 μL of serum-free DMEM containing 0.4 μg of DNA plasmids (negative control) or an equal amount of DNA–CdS (three syntheses). An equal amount of DNA–Lipofectamine 2000 complex prepared according to the manufacturer's instructions was used as a positive control. After 5 h incubation at 37 °C, the medium was replaced with 500 μL of fresh DMEM and the cells were incubated at 37 °C for 48 h to allow EGFP expression. For endosomal escape studies, DMEM containing DNA–CdS and 100 μM chloroquine was used for cell incubation. The EGFP expression was observed on a Leica TCS SP5 confocal laser scanning microscope using a 63$\times$ oil immersion objective with 488 nm argon laser excitation, and the emission signal was collected between 500 and 550 nm. The relative transfection efficiency was determined by dividing the number of DNA–CdS-transfected 293T cells with EGFP expression by the number of DNA–Lipo-transfected 293T cells with EGFP expression. The absolute transfection efficiency was defined as the percentage of 293T cells with EGFP expression. Ten fields of view (63$\times$ objective) including approximately 500 cells were analyzed to calculate the absolute transfection efficiencies under each condition. Three fields of view (20$\times$ objective) including approximately 1000 cells were analyzed to calculate the relative transfection efficiencies under each condition. Three trials were conducted for each transfection condition, and the standard deviations (uncertainty) are below 10% for all the calculated transfection efficiencies.

Cytotoxicities of DNA–CdS Hybrid Nanostructures. 293T cells were cultured as described above. Aliquots (100 μL) were seeded (2 $\times$ 10^4 cells) into a 96-well plate (Costar). After overnight incubation, cell medium was replaced with 100 μL of serum-free DMEM containing 0.4 μg of DNA plasmids or an equal amount of DNA–CdS, and the cells were incubated at 37 °C for 5 h. Then the medium was replaced with 100 μL of fresh DMEM, and the cells were further incubated at 37 °C for 48 h. The medium was then replaced with 100 μL of DMEM containing 5 mg/mL MTT, and the cells were incubated at 37 °C for 4 h. Formazan crystals were dissolved in 100 μL of DMSO with gentle agitation for 10 min. Cells treated with medium alone and Triton X-100 were used as negative and positive controls, respectively. The absorbance of the supernatant at 490 nm was measured using a Biotek Synergy 4 plate reader.

PI Labeling and Co-localization. A 0.4 μg amount of DNA or an equal amount of DNA–CdS in 100 μL of serum-free DMEM was fluorescently labeled by 0.16 μg of PI and then incubated with 293T cells for 5 h at 37 °C. Cells were then washed twice with 1$\times$ PBS and imaged on a Leica TCS SP5 confocal laser scanning microscope with 543 nm argon laser excitation, and the emission signal was collected between 590 and 700 nm. Equal amounts of PI-labeled naked DNA plasmids and DNA–Lipofectamine 2000 complex were used as negative and positive controls, respectively. The parameters for signal collections were set constant for all the samples. Mean fluorescence intensities of cells were quantified using ImageJ software. For co-localization studies, the cells were incubated with 100 μL of Lysotracker Green DND-26 solution for 30 min right before confocal microscopy experiments. Localization of Lysotracker Green DND-26 was visualized with 488 nm argon laser excitation, and the emission signal was collected between 500 and 550 nm.

Agarose Gel Electrophoresis. Agarose gel electrophoresis was performed on a DYY-6C electrophoresis apparatus (Beijing Liuyi Instrument Factory). The electrophoresis was carried out on a 0.7% agarose gel at 120 V for 50 min. The gel was stained with SYBR Safe DNA gel stain (Invitrogen) and imaged on a Wealtec Dolphin-doc Plus gel imager. TA buffer (Tris and acetic acid) was used as the electrophoresis buffer.

Acknowledgment. This work was supported in part by National Science Foundation of China (21175147), The Recruitment Program of Global Young Experts (1000-Young Talents Plan), and startup funds from Shenzhen Institutes of Advanced Technology, Chinese Academy of Sciences.

Supporting Information Available: Figures S1–S7. This material is available free of charge *via* the Internet at http://pubs.acs.org.

REFERENCES AND NOTES

1. Ma, N.; Tikhomirov, G. A.; Kelley, S. O. Nucleic Acid-Passivated Semiconductor Nanocrystals: Biomolecular Templating of Form and Function. *Acc. Chem. Res.* **2010**, *43*, 173–180.
2. Nam, K. T.; Kim, D.-W.; Yoo, P. J.; Chiang, C.-Y.; Meethong, N.; Hammond, P. T.; Chiang, Y.-M.; Belcher, A. M. Virus-Enabled Synthesis and Assembly of Nanowires for Lithium Ion Battery Electrodes. *Science* **2006**, *312*, 885–888.
3. Douglas, T.; Young, M. Viruses: Making Friends with Old Foes. *Science* **2006**, *312*, 873–875.
4. Guli, M.; Lambert, E. M.; Li, M.; Mann, S. Template-Directed Synthesis of Nanoplasmonic Arrays by Intracrystalline Metalization of Cross-Linked Lysozyme Crystals. *Angew. Chem., Int. Ed.* **2010**, *49*, 520–523.
5. de la Rica, R.; Matsui, H. Applications of Peptide and Protein-Based Materials in Bionanotechnology. *Chem. Soc. Rev.* **2010**, *39*, 3499–3509.
6. de la Rica, R.; Matsui, H. Urease as Nanoreactor for Growing Crystalline ZnO Nanoshells at Room Temperature. *Angew. Chem., Int. Ed* **2008**, *47*, 5415–5417.
7. Ma, N.; Marshall, A. F.; Rao, J. Near-Infrared Light Emitting Luciferase *via* Biomineralization. *J. Am. Chem. Soc.* **2010**, *132*, 6884–6885.
8. Ma, N.; Sargent, E. H.; Kelley, S. O. Biotemplated Nanostructures: Directed Assembly of Electronic and Optical Materials Using Nanoscale Complementarity. *J. Mater. Chem.* **2008**, *18*, 954–964.
9. Berti, L.; Burley, G. A. Nucleic Acid and Nucleotide-Mediated Synthesis of Inorganic Nanoparticles. *Nat. Nanotechnol.* **2008**, *3*, 81–87.
10. Ma, N.; Yang, J.; Stewart, K. M.; Kelley, S. O. DNA-Passivated CdS Nanocrystals: Luminescence, Bioimaging, and Toxicity Profiles. *Langmuir* **2007**, *23*, 12783–12787.
11. Ma, N.; Dooley, C. J.; Kelley, S. O. RNA-Templated Semiconductor Nanocrystals. *J. Am. Chem. Soc.* **2006**, *128*, 12598–12599.
12. Hinds, S.; Taft, B. J.; Levina, L.; Sukhovatkin, V.; Roy, M. D.; Dooley, C. J.; Roy, M. D.; Sargent, E. H.; Kelley, S. O. Nucleotide-Directed Growth of Semiconductor Nanocrystals. *J. Am. Chem. Soc.* **2006**, *128*, 64–65.
13. Ma, N.; Sargent, E. H.; Kelley, S. O. One-Step DNA-Programmed Growth of Luminescent and Biofunctionalized Nanocrystals. *Nat. Nanotechnol.* **2009**, *4*, 121–125.
14. Rejman, J.; Oberle, V.; Zuhorn, I. S.; Hoekstra, D. Size-Dependent Internalization of Particles *via* the Pathways of Clathrin- and Caveolae-Mediated Endocytosis. *Biochem. J.* **2004**, *377*, 159–169.
15. Yu, W. W.; Qu, L.; Guo, W.; Peng, X. Experimental Determination of the Extinction Coefficient of CdTe, CdSe, and CdS Nanocrystals. *Chem. Mater.* **2003**, *15*, 2854–2860.
16. Xu, Y.; Szoka, F. C. Mechanism of DNA Release from Cationic Liposome/DNA Complexes Used in Cell Transfection. *Biochemistry* **1996**, *35*, 5616–5623.

17. Erbacher, P.; Roche, A. C.; Monsigny, M.; Midoux, P. Putative Role of Chloroquine in Gene Transfer into a Human Hepatoma Cell Line by DNA/Lactosylated Polylysine Complexes. *Exp. Cell Res.* **1996**, *225*, 186–194.
18. Ho, Y.-P.; Chen, H. H.; Leong, K. W.; Wang, T.-H. Evaluating the Intracellular Stability and Unpacking of DNA Nanocomplexes by Quantum Dots-FRET. *J. Controlled Release* **2006**, *116*, 83–89.